

Human-Multirobot Collaborative Mobile Manipulation: the Omnid Mocobots

Matthew L. Elwin*, *Member*, Billie Strong*, *Member*, Randy A. Freeman, *Member*, and Kevin M. Lynch, *Fellow*

Abstract—The Omnid human-collaborative mobile manipulators are an experimental platform for testing control architectures for autonomous and human-collaborative multirobot mobile manipulation. An Omnid consists of a mecanum-wheel omnidirectional mobile base and a series-elastic Delta-type parallel manipulator, and it is a specific implementation of a broader class of mobile collaborative robots (“mocobots”) suitable for safe human co-manipulation of delicate, flexible, and articulated payloads. Key features of mocobots include passive compliance, for the safety of the human and the payload, and high-fidelity end-effector force control independent of the potentially imprecise motions of the mobile base. We describe general considerations for the design of teams of mocobots; the design of the Omnids in light of these considerations; manipulator and mobile base controllers to achieve useful multirobot collaborative behaviors; and initial experiments in human-multirobot collaborative mobile manipulation of large, unwieldy payloads. For these experiments, the only communication among the humans and Omnids is mechanical, through the payload.

Index Terms—swarm robotics, human-robot collaboration, physical human-robot interaction, multirobot systems.

I. INTRODUCTION

This paper introduces the Omnid mobile collaborative robot, or “mocobot” for short. The Omnid mocobots are designed specifically for team mobile manipulation, including autonomous cooperative manipulation and manipulation in collaboration with one or more human partners (Figure 1).

Here we focus on human-multirobot collaborative mobile manipulation, particularly factory, warehouse, or construction manipulation tasks with the following characteristics:

- 1) the payload is large and it is impractical for a single robot to manipulate it;
- 2) it is advantageous to have multiple contacts with the payload, either to minimize stress concentrations on a delicate payload or to control all the degrees of freedom of an articulated or flexible payload; and
- 3) the task is unique or difficult to automate, requiring the adaptability and situational awareness of one or more human collaborators.

Even if the task will be automated, a human-collaboration phase can be useful for human-guided machine learning.

Human-robot communication during collaboration can be verbal, visual, or physical, but we focus on physical human-robot interaction through the payload because the direct haptic interaction provides the human a high-bandwidth and intuitive communication channel for manipulation tasks [2]. In

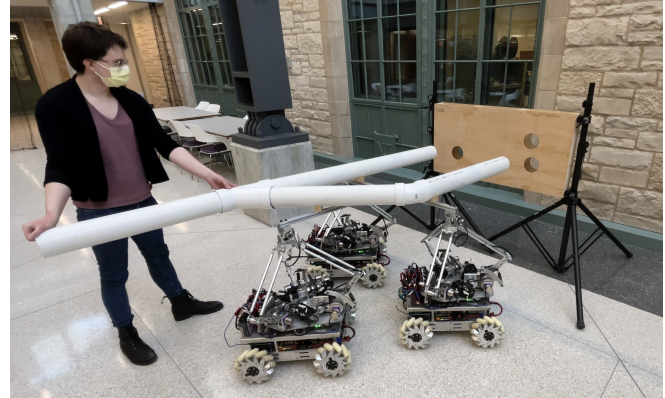


Fig. 1. A human and three Omnid mocobots performing 6-dof collaborative assembly of a bulky payload into a fixture.

well-designed human-mocobot collaborative manipulation, the forces required of the human should be small, and manipulation should be intuitive and safe.

The mocobots also communicate with each other mechanically through the payload. Future work will explore additional capabilities enabled by continuous wireless communication among the mocobots and/or a central base station.

For the safety of the human and the payload, mocobots should provide passive mechanical compliance to compensate for the limited bandwidth of active impedance controllers. Mocobots should also provide sufficient manipulability of the payload to enable effective autonomous or human-collaborative manipulation. We describe these and other design requirements for a team of mocobots (Section III); explain how the design of the Omnids, with their omnidirectional mobile bases and series-elastic parallel manipulators, satisfies these requirements (Section IV); present low-level controllers that facilitate useful collaborative behaviors (Section V); and describe experiments where the Omnids render large payloads weightless for easy collaborative manipulation by one or more human partners (Section VI). Videos of some of the experiments can be found in [1].

The Omnids are a platform for evaluating controllers for human-multirobot collaborative manipulation, not an industry-ready solution for multirobot manipulation. For example, the Omnid manipulators have a limited workspace and cannot autonomously grasp a payload—the payload is manually attached to the robots before each experiment. The control strategies described here, however, apply to other mocobot designs, including outdoor and legged mocobots, provided they satisfy the design criteria described in Section III.

*MLE and BS contributed equally to this work.

Video of some of the experiments in this paper can be found at <https://www.youtube.com/watch?v=SEuFfONryL0> [1].

II. RELATED WORK ON HUMAN-ROBOT COLLABORATIVE MANIPULATION

The ‘‘cobot’’ concept for human-robot collaborative manipulation was introduced in [3] and focused on ensuring operator safety through the use of programmable constraints. Optimal constraints for ergonomic human-cobot interaction, including collaborative mobile manipulation, are described in [4], [5].

Much previous work on human-robot collaborative manipulation has focused on active compliance and impedance control strategies for the robots and various methods for inferring the human’s intent. Kosuge et al. [6] describe the development of an early dual-arm mobile manipulator intended for human interaction called ‘‘MR Helper,’’ where each arm is a 7-DOF Mitsubishi PA-10 equipped with a six-axis wrist force-torque sensor. Many other single- and dual-arm mobile manipulators for human interaction have been developed, including bipeds participating in shared carrying of objects [7]–[10].

Approaches to human-robot physical collaboration include active compliance control for an anthropomorphic robotic torso mounted on an omnidirectional robot base [11], impedance control [12], and the identification of a discrete set of load-sharing policies between the human and the robot [13]. Some benefit has been observed for allowing humans and robots to dynamically exchange leader and follower roles during co-manipulation [14], [15]. In [16], the robot adapts its strategy based on the human’s willingness to adapt their strategy: when the human is willing to adapt, the robot attempts to guide the human to a strategy it believes is optimal, but when the human is not willing to adapt, the robot assigns the leader role to the human to retain trust. Machine learning has also been applied to infer human intent during cooperative manipulation [17]–[19].

The preceding work focuses on single-human single-robot mobile manipulation, and there has been little prior work on human-multirobot mobile manipulation. Notable exceptions include systems designed for multirobot autonomous mobile manipulation but modified to replace the robot leader with a human leader. In [20], a human leads a multirobot system manipulating an object via formation control, directing the motion remotely with the assistance of vibrotactile feedback. In [21], the human teleoperates the leader robot or physically grabs the co-manipulated object, and the leader’s force is amplified by the other robots in the team.

III. DESIGN CONSIDERATIONS FOR A MOCOBOT TEAM

Many mobile manipulators consist of a wheeled mobile base with one or more robot arms (e.g., a UR16 [22] or a Franka Emika Panda [23]) mounted to it. When multiple mobile manipulators grasp a fragile payload, however, the safety of the load may be at risk due to mechanical overconstraint.

When multiple robots grasp a rigid payload, closed-loop constraints are introduced, which can be modeled by m holonomic constraints $f(q) = 0$, where $q \in \mathbb{R}^n$ is a set of generalized coordinates describing the configuration of the payload and the mobile manipulators. Wheeled robots may also be subject to k nonholonomic constraints of the form $H(q)\dot{q} = 0$. The holonomic constraints can be differentiated

and combined with the nonholonomic constraints to obtain a complete set of Pfaffian constraints of the form $A(q)\dot{q} = 0$, and the dynamics of the multirobot-payload closed-chain can be written collectively in the form

$$M(q)\ddot{q} + c(q, \dot{q}) + p(q) = S(q)u(q) + A^\top(q)\lambda \quad (1)$$

$$A(q)\dot{q} = 0, \quad (2)$$

where $M(q) \in \mathbb{R}^{n \times n}$ is the combined mass matrix of the robots and the payload; $c(q, \dot{q}) \in \mathbb{R}^n$ is a vector of Coriolis, centripetal, and possibly mechanical damping generalized forces; $p(q) \in \mathbb{R}^n$ is a vector of generalized forces due to potential (e.g., gravity or springs); $u(q) \in \mathbb{R}^{n_a}$ is the n_a -vector of robot control forces and torques produced by a feedback controller (which is typically at least a function of q); $S(q) \in \mathbb{R}^{n \times n_a}$ is a transmission matrix mapping the controls to the generalized coordinates they act on; $A(q) \in \mathbb{R}^{(m+k) \times n}$ represents the Pfaffian constraints; and $\lambda \in \mathbb{R}^{m+k}$ is a set of generalized forces enforcing the constraints. See [23] for an example of such a model for multirobot manipulation.

One goal of the feedback law $u(q)$ could be to minimize components of the constraint forces λ associated with the grasps, avoiding large compressive or tensile internal forces on the payload. The simplified dynamics (1) do not distinguish, however, between passive mechanical forces (e.g., $p(q)$) and the active feedback-controlled forces $u(q)$, which are subject to limited bandwidth and possibly network latency. The non-idealities of active feedback control mean that incompatibilities of the motions of the end-effectors of the mocobots must be absorbed by unmodeled mechanical compliances in the robots or the payload itself. These mechanical compliances are often poorly understood.

A. Passive Compliance

For the safety of the payload and human collaborators, mocobots should implement well-characterized passive mechanical compliance. This compliance may be achieved by passive elements (e.g., springs) or actuators such as direct-drive actuators, series-elastic actuators (SEAs), variable stiffness actuators (VSAs), or variable impedance actuators (VIAs). The i th mocobot locally exhibits a passive linear stiffness

$$\delta \mathcal{F}_i = K_i \delta X_i$$

at its end-effector, where the (possibly configuration-dependent) positive-semidefinite stiffness matrix $K_i \in \mathbb{R}^{6 \times 6}$ maps $\delta X_i \in \mathbb{R}^6$ (a differential change in the exponential coordinates describing the configuration of the end-effector) to $\delta \mathcal{F}_i \in \mathbb{R}^6$ (a differential change in wrench), where X_i and \mathcal{F}_i are expressed in a common frame. If N mocobots grasp a rigid payload, the total stiffness of the payload can be expressed in a common payload frame as

$$K = \sum_{i=1}^N [\text{Ad}_{T_{ip}}]^\top K_i [\text{Ad}_{T_{ip}}], \quad (3)$$

where $T_{ip} \in SE(3)$ expresses the configuration of the payload relative to the i th end-effector frame.

The safety of a payload to position perturbations at each end-effector places an upper bound on each end-effector’s

passive stiffness K_i (e.g., on the maximum eigenvalue of K_i), and the safety of a collaborating human places an upper bound on the total stiffness K of the payload. Lower bounds on each end-effector's stiffness may come from responsiveness requirements of some control modes (e.g., motion control).

B. Manipulability

Manipulability analysis can be used to understand which payload degrees-of-freedom a mocobot team can control. Differentiating Equation (2), substituting into Equation (1), and eliminating the constraint forces λ yields

$$\ddot{q} = F(q)u + g(q, \dot{q}), \quad (4)$$

where, after dropping the dependence on q for brevity,

$$F = M^{-1}(I - A^T(AM^{-1}A^T)^{-1}AM^{-1})S. \quad (5)$$

The full configuration $q \in \mathbb{R}^n$ can be decomposed as $q = [q_p^T \ q_r^T]^T$, where $q_p \in \mathbb{R}^{n_p}$ and $q_r \in \mathbb{R}^{n_r}$ are generalized coordinates of the payload and robots, respectively, and $n = n_p + n_r$. If the payload is a rigid body, then $n_p = 6$, and if the payload is articulated with d internal degrees of freedom, then $n_p = 6 + d$.

Accordingly, the matrix $F(q)$ from Equation (1) becomes

$$F(q) = \begin{bmatrix} F_p(q) \\ F_r(q) \end{bmatrix},$$

where $F_p(q) \in \mathbb{R}^{n_p \times n_a}$ and $F_r(q) \in \mathbb{R}^{n_r \times n_a}$. This matrix relating controls u to accelerations \ddot{q} depends on the configuration of the payload q_p and the robots' configuration q_r , which determines their grasp locations on the payload. We define the linear *manipulability* of the payload at q as $\text{rank}(F_p(q))$, the number of degrees of freedom of the payload that can be instantaneously independently controlled. We say that the payload is fully manipulable at q if $\text{rank}(F_p(q)) = n_p$.

C. Manipulation Force Control Independent of Mobile Base Motion Control

The mobile base of a mocobot ideally keeps its manipulator near the center of its workspace throughout the manipulation, for maximum dexterity. We assume the mobile base is motion controlled, perhaps imprecisely. For example, wheels may slip or skid; the footholds of a legged mobile base may be uncertain or yielding; and the ground may be uneven.

Conversely, we require the mocobot to be capable of predictable compliance and force control at its end-effector, effectively independent of the motion of the mobile base, for the safety of the human and the payload.

Thus the mechanical design and control of the mocobot should support reasonable decoupling between imprecise motion control of the mobile base and the force-controlled behavior visible at the end-effector. With this abstraction enforced by design and/or low-level control behaviors, mocobots of different designs (wheeled, tracked, legged, etc.) may implement the same high-level coordinated behaviors for human-collaborative and autonomous team manipulation. Below we describe how the Omnid mocobot effectively implements force control at its end-effector.

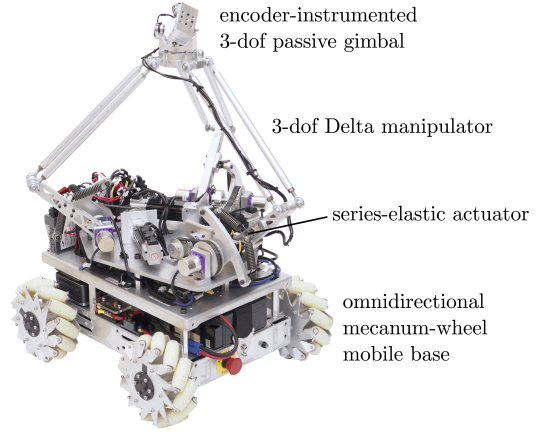


Fig. 2. An Omnid mocobot, consisting of an omnidirectional mobile base, a 3-dof SEA-driven Delta parallel manipulator, and a 3-dof passive gimbal.

# Omnids	end-effector configuration	payload manipulability
1	no constraints	$\text{rank}(F_p(q)) = 3$
2	not collocated	$\text{rank}(F_p(q)) = 5$
3	not collinear	$6 \leq \text{rank}(F_p(q)) \leq 9$

TABLE I
MANIPULABILITY OF THE PAYLOAD AS A FUNCTION OF THE NUMBER OF OMNIDS GRASPING THE PAYLOAD.

IV. DESIGN OF THE OMNID MOCOBOTS

The Omnid mocobots are designed to approximately decouple the force-controlled behavior at the end-effector from imprecise motion control of the mobile base (Section III-C), exhibit well-characterized passive compliance (Section III-A), and, with a team of three or more, achieve full manipulability of payloads with up to three internal degrees of freedom (Section III-B). The Omnids are specifically designed for team manipulation; a single Omnid is incapable of controlling all six degrees of freedom of a rigid payload.

Each Omnid consists of a mecanum-wheel omnidirectional mobile base and a 6-dof manipulator. The manipulator is a 3-dof Delta parallel mechanism [24] driven by SEAs plus an encoder-instrumented 3-dof passive gimbal “wrist” (Figure 2). Thus an Omnid has six independently-controlled degrees of freedom (two translational and one rotational freedom for the mobile base, plus three translational freedoms for the manipulator) and three passive rotational freedoms at the wrist.

With this design, each Omnid can apply three-dimensional linear forces that act on the payload at the center of each wrist. Assuming the end-effectors of Omnids collaboratively manipulating a payload are not at the boundaries of their workspaces, the manipulability of the payload as a function of the number of Omnids grasping the payload is given in Table I. If the gimbal centers of three collaborating Omnids are not collinear, they can locally actuate all six degrees of freedom of a rigid payload, plus up to a maximum of three additional internal degrees of freedom of an articulated payload. If the gimbals of the Omnids are collinear, they cannot resist torque about the line. At such a singularity, the manipulability of a rigid payload drops to 5.

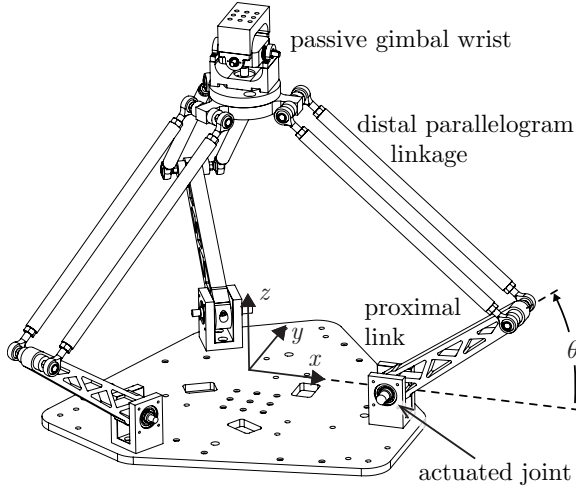


Fig. 3. The Omnid's manipulator is an SEA-driven Delta parallel mechanism plus a passive gimbal wrist. The gimbal center is at $x = (x, y, z)$ in the manipulator frame, which is centered between the actuated (proximal) joints.

SEA max continuous torque	9 Nm
SEA stiffness	60.1 Nm/rad
Delta proximal link length	0.200 m
Delta distal parallelogram linkage length	0.368 m
Joint limits at each proximal joint θ_i	$[-15^\circ, 100^\circ]$
Joint angles θ_i at home	36.6°
End-effector (x, y, z) position at home	$(0, 0, 0.420 \text{ m})$
Radius of workspace-inscribed sphere about home	0.15 m
End-effector max continuous force at home	90 N
End-effector linear stiffness K_{xx}, K_{yy} at home	1400 N/m
End-effector linear stiffness K_{zz} at home	2000 N/m
Theoretical end-effector position resolution at home	$0.3 \mu\text{m}$
Theoretical end-effector force resolution at home	$500 \mu\text{N}$

TABLE II

PHYSICAL PROPERTIES OF THE OMNID DELTA MANIPULATOR AND ITS THEORETICAL POSITION AND FORCE CAPABILITIES AT THE HOME CONFIGURATION.

A. Series-Elastic Delta Manipulator with Gimbal Wrist

The Omnid manipulator is a Delta parallel manipulator plus a passive gimbal wrist (Figure 3). Each of the three legs supporting the Delta's end-effector consists of a proximal revolute joint (driven by an SEA, described below) and a distal unactuated parallelogram linkage. Away from singularities of the mechanism, in the normal operating workspace of the wrist, the angles of the three proximal revolute joints $\theta = (\theta_1, \theta_2, \theta_3)$ map to the three translational coordinates $x = (x, y, z)$ of the center of the gimbal wrist, expressed in a frame fixed to the manipulator's base, through the forward kinematics $x = h(\theta)$. The Jacobian $J(\theta) = \partial h / \partial \theta \in \mathbb{R}^{3 \times 3}$ is full rank in this region and satisfies $\dot{x} = J(\theta)\dot{\theta}$ and $\dot{\theta} = J^{-1}(\theta)\dot{x}$. The physical parameters of the Omnid SEA Delta manipulator are given in Table II.

Each SEA consists of a brake-equipped Applied Motion Products J0100-353-3-000 motor with 40PE025 25:1 planetary gearhead, followed by a toothed belt reduction of 12:7 driving a revolute joint that couples to the Delta's proximal revolute joint by two antagonistic linear extension springs (Figure 4). This setup creates a joint with a maximum continuous torque of approximately 9 Nm and a highly linear torsional stiffness,

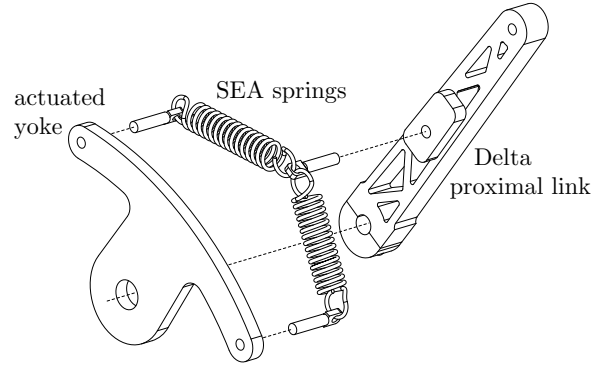


Fig. 4. The custom SEA at each proximal joint of the Delta manipulator consists of a yoke driven by a geared motor and two antagonistic linear extension springs.

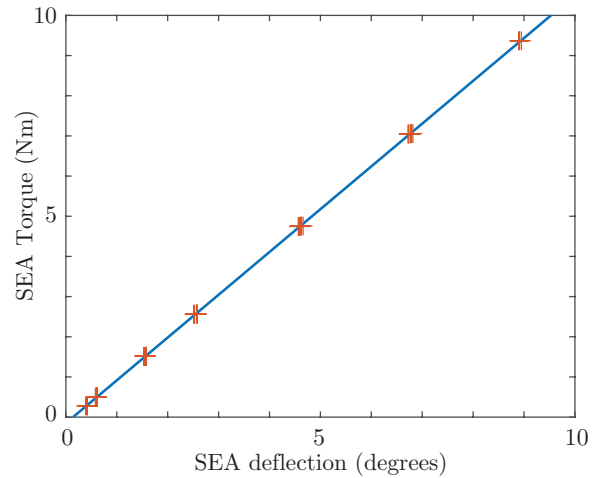


Fig. 5. Experimental SEA torque as a function of deflection (actuator angle minus the proximal joint angle) and a near-perfect linear fit to the data.

approximately $k_i = 60.1 \text{ Nm/rad}$ (Figure 5). Defining the matrix $K_\theta = \text{diag}(k_i, k_i, k_i) \in \mathbb{R}^{3 \times 3}$, the configuration-dependent linear stiffness at the gimbal wrist is given by $K(\theta) = J^{-\top}(\theta)K_\theta J^{-1}(\theta)$. The maximum continuous end-effector force and the stiffness at the home configuration are given in Table II.

The angles of the driving joint and the Delta proximal joint (before and after the springs, respectively) are measured by Broadcom AS38-H39E-S13S 23-bit absolute encoders. Joint torque is estimated by multiplying the joint stiffness by the angular difference between these joints, resulting in a theoretical resolution of approximately $45 \mu\text{Nm}$. See Table II for the resulting end-effector position and force resolution at the home configuration.

The accurate force sensing and control of the SEA Delta manipulator achieves the desired decoupling of end-effector forces from the motion of the mobile base (Section III-C).

The freely-rotating gimbal wrist prevents transmission of torques about the gimbal center. The three angles of the gimbal $\alpha = (\alpha_x, \alpha_y, \alpha_z)$ are measured by CUI AMT213A-V capacitive 12-bit absolute encoders. If the end-effector is attached to a rigid payload, and the location of the end-

effector frame relative to the payload frame is known, then the configuration of the payload relative to the Omnid's mobile base is known from the six encoders of the Delta and gimbal.

B. Omnidirectional Mobile Base

The omnidirectional mobile base is a modified SuperDroid IG52-DB4 platform driven by four mecanum wheels. Each wheel is driven in velocity-control mode by an encoder-instrumented motor with a gearbox and belt drive. The encoders enable odometry which approximately tracks the incremental motion of the mobile base. For global positioning, an overhead camera can track the payload and/or mobile base, or the mobile base may be equipped with Intel T265 cameras. Global positioning is not needed for many collaborative manipulation modes, however.

C. Computing and Communication

Each Omnid is equipped with several TM4C123GH6PM microcontrollers. The Delta manipulator has a top-level microcontroller to perform kinematics and whole-arm control at 100 Hz. Each SEA joint has its own microcontroller to implement low-level torque control at 800 Hz, and the gimbal has a microcontroller to measure the gimbal joint angles. The top-level Delta microcontroller communicates with the four other microcontrollers via dedicated RS-485 buses.

The mobile base uses three microcontrollers: one for the mobile base controller and one each for low-level control of the front and rear wheels, respectively. The top-level controller communicates with the wheel controllers via RS-485.

The top-level Delta and mobile base microcontrollers communicate via RS-485 with an Intel NUC7i7BNH PC running Linux and ROS Noetic [25], which handles wifi communication among robots and a base station. Control modes described in this paper do not require wireless communication.

V. OMNID BEHAVIORS AND CONTROL

The high-level control system for each Omnid robot is illustrated in Figure 6. There are two major controllers: the manipulator controller and the mobile base controller.

The manipulator controller calculates the commanded end-effector force f_{com} as a function of the manipulator's configuration $q_{\text{manip}} = (\theta, \alpha)$ relative to the mobile base and optionally the payload and mobile base's configurations. The torques commanded at the individual SEAs are $\tau = J^T(\theta)f_{\text{com}}$.

The mobile base controller calculates the commanded chassis-frame planar twist of the mobile base \mathcal{V}_{com} as a function of q_{manip} and optionally the payload and mobile base's configurations. The commanded wheel velocities $w \in \mathbb{R}^4$ are calculated as $w = H\mathcal{V}_{\text{com}}$, where $H \in \mathbb{R}^{4 \times 3}$ is determined by the radius of the wheels and their configuration relative to the chassis frame [24].

A. Individual Omnid Behaviors

Below we describe manipulator and mobile base controllers that implement useful behaviors for a single Omnid. These same controllers are building blocks for multi-Omnid collaboration.

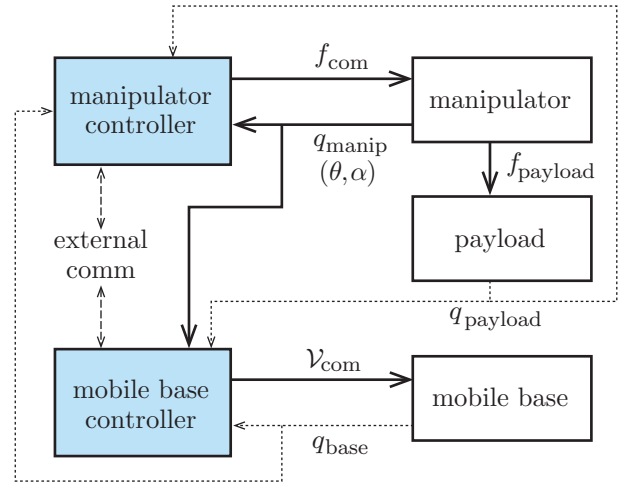


Fig. 6. Overview of each Omnid's high-level control system. The dashed lines indicate optional communication with a centralized controller or other Omnids. The dotted lines indicate optional exteroceptive sensing of the payload and mobile base configurations.

1) Manipulator Control Modes:

a) *Manipulator Locked Mode:* In this mode, the SEA brakes are locked, and the manipulator provides an instrumented passive spring for translations and an instrumented freely-rotating gimbal for orientation.

b) *Manipulator Float Mode:* In this mode, the manipulator exerts a force to cancel its own weight. The joint-space mass matrix of the manipulator is $M(\theta, \alpha) \in \mathbb{R}^{3 \times 3}$, which can be expressed in the (x, y, z) task space as $\Lambda(\theta, \alpha) = J^{-T}(\theta)M(\theta, \alpha)J^{-1}(\theta)$. In manipulator float mode, the commanded end-effector force is

$$f_{\text{com}} = -\Lambda(\theta, \alpha) \begin{bmatrix} 0 \\ 0 \\ \mathbf{g} \end{bmatrix},$$

the force needed to cancel the effect of the gravitational acceleration \mathbf{g} in the z direction. If the end-effector approaches the boundary of a sphere conservatively inscribed in its workspace, a spring force is added to the float force to push the end-effector away from the boundary.

Float mode may be augmented with an optional deadband behavior emulating static Coulomb friction. If the operator brings the end-effector to rest, the end-effector remains at rest until a minimum force is applied to initiate motion.

c) *Manipulator Plus Payload Float Mode:* This mode builds upon float mode, but also accounts for the additional mass of a payload. If several Omnids manipulate a common payload, and each Omnid is able to continuously calculate the component of the payload's mass that it supports, this mode floats the entire payload. Human interaction with the payload is as if the payload is in zero gravity.

d) *Manipulator Force, Motion, and Impedance Control:* Each of force, motion, and impedance control compute an end-effector force to add to the force computed by the gravity compensation of the float modes.

To achieve a desired linear force $f_d \in \mathbb{R}^3$ at the wrist, the commanded SEA joint torques are $\tau = J^T(\theta)f_{\text{com}}$, where $f_{\text{com}} = f_d + f_{\text{float}}$, and f_{float} is the gravity-compensating force calculated by a float mode. An 800 Hz PID controller drives the SEAs to achieve the commanded torques.

A PID controller computes the added end-effector force for motion control. Other standard trajectory controllers are also possible [24].

The manipulator can also be controlled to emulate desired linear mass-spring-damper impedance properties at the wrist,

$$f_d = M(\ddot{x}_d - \ddot{x}) + B(\dot{x}_d - \dot{x}) + K(x_d - x).$$

This feedback-controlled behavior is only effective at low frequencies; at higher frequencies, the passive mechanical properties of the manipulator dominate the impedance.

Since the manipulator has three controlled linear degrees of freedom, each of M , B , and K is a symmetric 3×3 matrix.¹ Due to symmetry, each matrix is fully specified by six entries: three on the diagonal and three cross-coupling terms. For stability, we restrict these matrices to be positive definite, and we typically focus on stiffness and damping only.

2) Mobile Base Control Modes:

a) *Mobile Base Recentering Control*: Under recentering control, the mobile base moves to keep the horizontal (x, y) coordinates of the wrist and the gimbal angle α_z near zero. This ensures maximum range of motion of the manipulator to implement high-bandwidth force control. To drive (x, y, α_z) to zero, we use a PD controller to calculate a planar twist $\mathcal{V}_{\text{com}} \in \mathbb{R}^3$ for the mobile base.

b) *Mobile Base Motion Control*: This mode refers to any standard motion controller (e.g., [24]) to drive the mobile base along a desired trajectory, using either odometry, onboard localization, or external sensing for position feedback.

c) *Mobile Base Motion Plus Recentering Control*: In this control mode, the mobile base's commanded motion is

$$\mathcal{V}_{\text{com}} = \alpha\mathcal{T} + (1 - \alpha)\mathcal{R}, \quad 0 \leq \alpha \leq 1,$$

where \mathcal{T} is a motion controller and \mathcal{R} is the recentering controller. When $\alpha = 1$, the mobile base attempts to follow a desired trajectory regardless of the manipulator configuration. When $\alpha = 0$, the mobile base implements recentering control. For intermediate values, the mobile base attempts to follow a desired trajectory while also complying to deflections of the manipulator from its home configuration. The value of α may be chosen to approach zero as the manipulator approaches the boundary of its workspace.

3) *Behaviors Arising from the Combination of Manipulator and Mobile Base Controllers*: Certain combinations of the manipulator and mobile base controllers lead to useful behaviors of the entire Omnid. For example, manipulator float control plus mobile base recentering control yields a “walk the dog” behavior, allowing a user to easily push or pull an Omnid using light forces at the wrist.

¹Because wrist orientation is also measured, it is possible to implement 3×6 M , B , and K matrices to couple wrist orientations to linear forces.

B. Multi-Omnid Behaviors

Multi-Omnid behaviors may be classified into the following categories: emergent, emergent with coordinated initialization, distributed coordination, and centralized coordination.

Emergent behaviors use no explicit wireless communication between the Omnids or a centralized controller. The only interaction is mechanical, through the payload.

One useful emergent behavior occurs when each Omnid grasps a common payload and implements mobile base recentering control and manipulator stiffness control. If the virtual springs are sufficiently stiff in the vertical direction, the manipulators support the weight of the payload. The horizontal stiffnesses of the manipulators can be significantly lower, or zero, to minimize internal forces on the payload. In this mode, a human operator can easily transport rigid-body or articulated loads by pushing or pulling it.

An example of an emergent behavior with coordinated initialization is float control of a rigid-body payload using three Omnids. Each Omnid rigidly grasps the payload and initially knows the location of the payload's center-of-mass frame relative to each Omnid's end-effector frame.² Each Omnid can then determine the payload's relative configuration, and the portion of the payload's mass the manipulator supports, using only its manipulator's encoder information. When each Omnid implements recentering control of the mobile base and manipulator-plus-payload-float mode, the Omnids render the payload weightless, allowing easy human manipulation.

In contrast to emergent behaviors, coordinated behaviors involve wireless communication among the Omnids (distributed coordination) or among the Omnids and a central control station (centralized coordination). An example of a coordinated behavior is jiggling an articulated payload to determine its kinematic and inertial properties. We do not investigate coordinated behaviors in this paper.

VI. VALIDATION AND DEMONSTRATION

See [1] for videos of some of the demonstrations described below.

A. SEA Performance

Static torque measurement accuracy: Static load tests of the SEA indicate that the worst-case error in torque measurement is within $\pm 2\%$ of the full-scale continuous torque range of ± 9 Nm.

Static torque measurement precision: Any change in torque of 0.01 Nm (0.1% full scale) or greater is reliably detected.

SEA torque control step and frequency response: Figure 7 shows the measured 5 Nm step response of a single SEA for a blocked proximal link. The step response settling time is less than 0.1 s. Figure 8 shows the frequency response to small torque oscillations about a 5 Nm DC offset. Under these conditions, the bandwidth is between 20 and 30 Hz.

²Alternatively, the robots may perform a cooperative estimation procedure to determine this information.

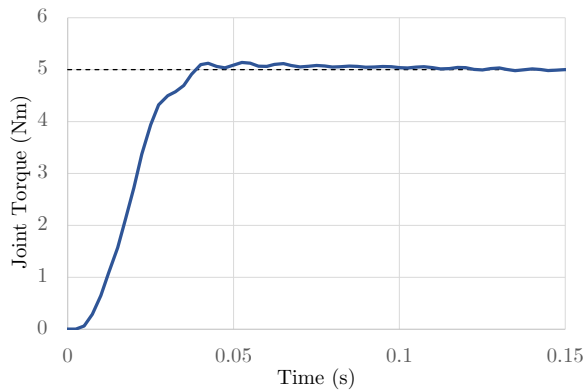


Fig. 7. Experimental step response of a blocked SEA joint to a 5 Nm torque command.

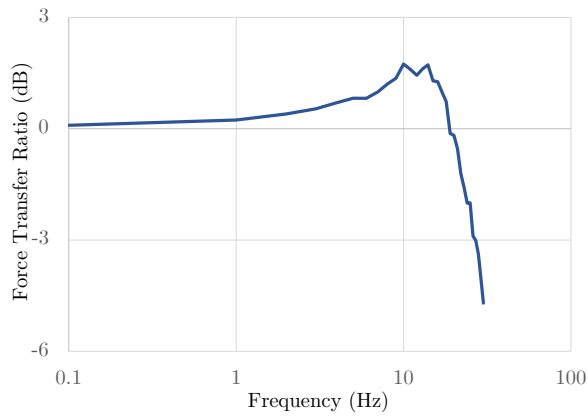


Fig. 8. Empirical frequency response of a blocked SEA joint to a ± 1 Nm sinusoidal torque command about a DC offset of 5 Nm.

B. Single-Omnid Experiments

Static load tests using weights at the end-effector of an Omnid indicate a worst-case force-sensing error of $\pm 2\%$ relative to the manipulator’s maximum continuous force of ± 90 N at the home configuration.

In the ideal manipulator plus payload float mode, a stationary wrist would begin to move in response to any nonzero applied force. In practice, friction causes a deadband where no motion occurs in response to small horizontal forces. With the manipulator near its home configuration and a payload of approximately 5 kg, motion typically occurs at less than 1 N of applied force.

Figure 9 shows the “walk the dog” Omnid behavior, where the manipulator implements float mode and the mobile base implements recentering control. In this mode, the human operator easily moves the mobile base in three degrees of freedom using only a light touch.

C. Multi-Omnid Single-Human Collaborative Assembly of a Rigid Payload

In this experiment (Figure 1), a single human and three Omnids collaboratively manipulate a rigid PVC pipe assembly weighing 15.6 kg, significantly more than a single Omnid’s 9 kg capacity at the manipulator’s home configuration. The



Fig. 9. “Walk the dog”: manipulator float mode plus mobile base recentering control allows a human operator to easily move the Omnid with a light touch.



Fig. 10. Two humans and three Omnids collaboratively manipulating a jointed payload (seven total degrees of freedom) among obstacles.

Omnid manipulators perform manipulator plus payload float mode and the mobile bases implement recentering control.

In this mode, the pipes feel weightless to the human. In a 6-dof assembly task, where two pipes are inserted into holes with a 2 mm tolerance, insertion is accomplished quickly with small operator forces (see [1]).

This Omnid behavior is an example of an emergent behavior with coordinated initialization. To correctly implement payload gravity compensation, each robot must be initialized with the attachment point of each Omnid manipulator relative to the payload’s center of mass. This information allows each Omnid to calculate the portion of the payload’s weight it supports. An alternative, not explored here, is to allow the Omnids to communicate wirelessly and estimate this information instead of providing it at initialization.

D. Multi-Omnid Multi-Human Collaborative Manipulation of an Articulated Payload

Figure 10 shows two humans and three Omnids collaboratively manipulating an articulated payload among obstacles. The payload has seven total degrees of freedom: six for one rigid body and one for the hinge joint. Three Omnids are sufficient to autonomously manipulate this payload (Table I), but a singularity occurs if the three wrists are brought into

alignment: the Omnids cannot generate a torque about the line, so the human operators must provide it.

In this task, each mobile base implements recentering control. Since each Omnid does not know the configuration of the payload or the other Omnids, the manipulator controller cannot exactly cancel gravity. Instead, on startup, each Omnid weighs the load on its manipulator and then provides a force to cancel that load throughout the rest of the manipulation. Forces from a virtual spring are added in the z -direction. The setpoint (zero-force) location for this virtual spring is the original z location of the end-effector. If the end-effector moves in z beyond a small threshold, the setpoint moves toward the end-effector, which simulates an object being dragged by a spring on a surface with Coulomb friction. This helps the user maintain and change the payload's height.

In the horizontal directions, the manipulator exhibits zero or low stiffness. An additional inward-pointing virtual spring is active only at the boundary of the workspace.

In this control mode, one or two human operators can easily control all seven degrees of freedom of the articulated payload. This multi-Omnid collaborative behavior is an example of an emergent behavior without coordinated initialization.

VII. FUTURE WORK

Our initial work shows that one or more humans can easily manipulate large, awkward, and articulated payloads in collaboration with a team of passively-compliant Omnid mocobots. Mocobot controllers that enable this collaboration are recentering control of the mobile base and gravity compensation and impedance control of the manipulator.

This paper describes initial demonstrations of Omnid human-collaborative capabilities. Future work will include the following three thrusts: (1) performance studies of transport and assembly tasks by naïve and experienced human users under different control schemes, such as teleoperation and direct human-payload physical interaction, to further explore the benefits of haptic interaction; (2) advanced collaboration capabilities enabled by wireless communication between the mocobots, such as estimation of human intent and implementation of control-barrier-function safety filters [26] for the human and the payload; and (3) autonomous multirobot manipulation, including estimation of payload kinematic and inertial properties and payload-centric wrench and impedance control for assembly tasks.

REFERENCES

- [1] M. L. Elwin, B. Strong, R. A. Freeman, and K. M. Lynch, "Human-multirobot collaborative mobile manipulation: the Omnid mocobots (video)," <https://www.youtube.com/watch?v=SEuFFONryL0>, 2022.
- [2] E. B. Küçüktabak, S. J. Kim, K. Lynch, and J. L. Pons, "Human-machine-human interaction in motor control and rehabilitation: a review," *Journal of NeuroEngineering and Rehabilitation*, vol. 18, no. 183, 2021.
- [3] J. E. Colgate, M. A. Peshkin, and W. Wannasuphprasit, "Cobots: Robots for collaboration with human operators," in *Proceedings of the ASME Dynamic Systems and Control Division*, 1996.
- [4] K. M. Lynch, C. Liu, A. Sorensen, S. Kim, M. Peshkin, J. E. Colgate, T. Tickel, D. Hannon, and K. Shiels, "Motion guides for assisted manipulation," *International Journal of Robotics Research*, vol. 21, no. 1, pp. 27–43, Jan. 2002.
- [5] P. Pan, M. A. Peshkin, J. E. Colgate, and K. M. Lynch, "Static single-arm force generation with kinematic constraints," *J Neurophysiology*, vol. 93, pp. 2752–2765, 2005.
- [6] K. Kosuge, M. Sato, and N. Kazamura, "Mobile robot helper," in *IEEE International Conference on Robotics and Automation*, 2000.
- [7] D. J. Agravante, A. Cherubini, A. Sherikov, P.-B. Wieber, and A. Kheddar, "Human-humanoid collaborative carrying," *IEEE Transactions on Robotics*, vol. 35, no. 4, pp. 833–846, Aug. 2019.
- [8] D. J. Agravante, A. Cherubini, A. Bussy, P. Gergondet, and A. Kheddar, "Collaborative human-humanoid carrying using vision and haptic sensing," in *IEEE International Conference on Robotics and Automation*, 2014.
- [9] A. Bussy, A. Kheddar, A. Crosnier, and F. Keith, "Human-humanoid haptic joint object transportation case study," in *IEEE/RSJ International Conference on Intelligent Robots and Systems*, 2012.
- [10] K. Yokoyama, H. Handa, T. Isozumi, Y. Fukase, K. Kaneko, F. Kanehiro, Y. Kawai, F. Tomita, and H. Hirukawa, "Cooperative works by a human and humanoid robot," in *IEEE International Conference on Robotics and Automation*, 2003.
- [11] J. Stückler and S. Behnke, "Following human guidance to cooperatively carry a large object," in *2011 11th IEEE-RAS International Conference on Humanoid Robots*, Oct 2011, pp. 218–223.
- [12] D. D. Carli, E. Hohert, C. A. C. Parker, S. Zoghbi, S. Leonard, E. Croft, and A. Bicchi, "Measuring intent in human-robot cooperative manipulation," in *IEEE Workshop on Haptic Audio Visual Environments and Games*, 2009.
- [13] M. Lawitzky, A. Mörtl, and S. Hirche, "Load sharing in human-robot cooperative manipulation," in *19th International Symposium in Robot and Human Interactive Communication*, Sep. 2010, pp. 185–191.
- [14] A. Mortl, M. Lawitzky, A. Kucukyilmaz, M. Segin, C. Basdogan, and S. Hirche, "The role of roles: physical cooperation between humans and robots," *International Journal of Robotics Research*, vol. 31, no. 13, pp. 1656–1674, 2012.
- [15] P. Evrard and A. Kheddar, "Homotopy switching model for dyad haptic interaction in physical collaborative tasks," in *World Haptics*, 2009.
- [16] S. Nikolaidis, A. Kuznetsov, D. Hsu, and S. Srinivasa, "Formalizing human-robot mutual adaptation: a bounded memory model," in *Human-Robot Interaction*, 2016.
- [17] E. Berger, D. Vogt, N. Haji-Ghassemi, B. Jung, and H. B. Amor, "Inferring guidance information in cooperative human-robot tasks," in *2013 13th IEEE-RAS International Conference on Humanoid Robots (Humanoids)*, Oct 2013, pp. 124–129.
- [18] E. Berger, M. Sastuba, D. Vogt, B. Jung, and H. Ben Amor, "Dynamic mode decomposition for perturbation estimation in human robot interaction," in *The 23rd IEEE International Symposium on Robot and Human Interactive Communication*, Aug 2014, pp. 593–600.
- [19] J. Lanini, H. Razavi, J. Urain, and A. Ijspeert, "Human intention detection as a multiclass classification problem: application in physical human-robot interaction while walking," *Robotics and Automation Letters*, vol. 3, no. 4, pp. 4171–4178, Oct. 2018.
- [20] D. Sieber, S. Music, and S. Hirche, "Multi-robot manipulation controlled by a human with haptic feedback," in *IEEE/RSJ International Conference on Intelligent Robots and Systems*, 2015.
- [21] Z. Wang and M. Schwager, "Force-amplifying n-robot transport system (force-ants) for cooperative planar manipulation without communication," *The International Journal of Robotics Research*, vol. 35, no. 13, pp. 1564–1586, 2016. [Online]. Available: <https://doi.org/10.1177/0278364916667473>
- [22] A. Giammarino, J. M. Gandarias, P. Balatti, M. Leonori, M. Lorenzini, and A. Ajoudani, "Super-man: Supernumerary robotic bodies for physical assistance in human-robot conjoined actions," 2022, <https://arxiv.org/abs/2201.06365>.
- [23] Y. Ren, S. Sosnowski, and S. Hirche, "Fully distributed cooperation for networked uncertain mobile manipulators," *IEEE Transactions on Robotics*, vol. 36, no. 4, pp. 984–1003, Aug. 2020.
- [24] K. M. Lynch and F. C. Park, *Modern Robotics: Mechanics, Planning, and Control*. Cambridge University Press, 2017, downloadable at <http://modernrobotics.org>.
- [25] M. Quigley, B. Gerkey, K. Conley, J. Faust, T. Foote, J. Leibs, E. Berger, R. Wheeler, and A. Ng, "ROS: an open-source robot operating system," in *Proc. of the IEEE Intl. Conf. on Robotics and Automation (ICRA) Workshop on Open Source Robotics*, Kobe, Japan, May 2009.
- [26] P. Wieland and F. Allgöwer, "Constructive safety using control barrier functions," *IFAC Proceedings Volumes*, vol. 40, no. 12, pp. 462–467, 2007, 7th IFAC Symposium on Nonlinear Control Systems.